Brian F. Knisely
Department of Mechanical Engineering,
The Pennsylvania State University,
University Park, PA 16802
e-mail: brian.knisely@carrier.com

Reid A. Berdanier[1]
Department of Mechanical Engineering,
The Pennsylvania State University,
University Park, PA 16802
e-mail: rberdanier@psu.edu

Joel H. Wagner
Department of Mechanical Engineering,
The Pennsylvania State University,
University Park, PA 16802
e-mail: jhw5315@psu.edu

Karen A. Thole
Department of Mechanical Engineering,
The Pennsylvania State University,
University Park, PA 16802
e-mail: kthole@psu.edu

Allan N. Arisi
Pratt & Whitney,
East Hartford, CT 06118
e-mail: allan.arisi@prattwhitney.com

Charles W. Haldeman
Pratt & Whitney,
East Hartford, CT 06118
e-mail: charles.haldeman@prattwhitney.com

Effects of Part-to-Part Flow Variations on Overall Effectiveness and Life of Rotating Turbine Blades

As firing temperatures in gas turbine engines continue to increase to achieve high efficiencies, components in the main gas path must be protected with cooling flows to ensure lifing targets are met. Manufacturing variations, however, influence the performance and life characteristics of components with the same nominal design. This study presents blade flow and overall cooling effectiveness measurements for nine true-scale, aero engine turbine blades with realistic manufacturing variations. Flow measurements were made through each blade at a fixed pressure ratio to determine flow variability between holes and between blades. Infrared thermography was used to capture spatially-resolved temperature measurements reported as overall effectiveness on the same nine blades under high-speed rotating conditions at the Steady Thermal Aero Research Turbine Laboratory. Thermal performance was correlated with blade flow performance indicating substantial blade-to-blade variations resulting from manufacturing differences. Measurements also indicated wide variations in cooling jet trajectories as well as overall cooling effectiveness. Finally, the observed blade-to-blade variations in effectiveness were scaled to engine conditions with lifing estimates showing some blades would be expected to last only half as long as others due to manufacturing variability. [DOI: 10.1115/1.4056679]

Keywords: heat transfer and film cooling, measurement techniques, infrared thermography, manufacturing variation, turbine blade and measurement advancements

Introduction

Improving the thermal efficiency of gas turbine engines is enabled by higher firing temperatures. Advances in turbine cooling technologies, including film cooling, have allowed hot section components to maintain designed part life and reliable operation. From experience, manufacturers know that significant variations in serviceable life can exist between parts with the same nominal design. Airfoils have been separated into classes for turbine wheel assembly based on geometric variations, but thermal variations should instead be used to reduce variations in blade life for a given engine. To manage variations, many cooling designs include a conservative approach to lifing by overcooling.

Variations in component lifing are expected in turbine operations given the tradeoffs between manufacturing costs and part tolerances [1]. When designers account for the variation associated with every design specification, the resulting system performance can be understood and modeled through statistics. This concept of "design for variation" (DFV) [2] provides a framework for maximizing part life and reliability for engine fleets. Before probabilistic models can be implemented as part of the design process, measurements are needed to determine the range of variations resulting from manufacturing as well as understand the sensitivity of thermal performance to each manufacturing factor.

Spatially-resolved surface temperature data on rotating blades provide a wealth of information to designers to achieve DFV. This paper uniquely quantifies observed variations in thermal performance of film cooling on rotating turbine blades and describes how cooling variations are correlated with flow variations that occur based on manufacturing differences. This paper is unique because it directly quantifies the manufacturing variations with resulting blade temperatures that are used to estimate blade lifing based on open literature lifing models.

Review of Literature

There are many factors that can affect component life in gas turbine engines. As described in detail by Balevic et al. [3], some of these factors include steady operation settings such as firing temperature, rotor speed, and fuel type; transient effects such as number of startup events and startup speed; and environmental effects such as ambient temperature, moisture, and air quality. Each of these factors affects the temperature distribution and corresponding life of rotor blades in different ways. For the scope of our paper, the sole effect of surface temperature on part life for blades under continuous operation is considered.

The relationship between surface temperature and corresponding part life is complex and dependent on a specific turbine design, but several researchers have provided first-order estimates. In general, part life is a nonlinear function with reported estimates of a 25–40 °C increase in surface temperature resulting in a 50% reduction in life [4–6].

Few publications have provided analysis on the impact of surface temperature increases beyond the design target on blade life because the tools and procedures are proprietary to each engine company. Reyhani et al. [7] described a method for calculating blade life by modeling conjugate heat transfer, fatigue, creep, and fatigue-creep

[1]Corresponding author.

Contributed by the International Gas Turbine Institute (IGTI) of ASME for publication in the Journal of Turbomachinery. Manuscript received August 1, 2022; final manuscript received October 31, 2022; published online February 9, 2023. Tech. Editor: David G. Bogard.

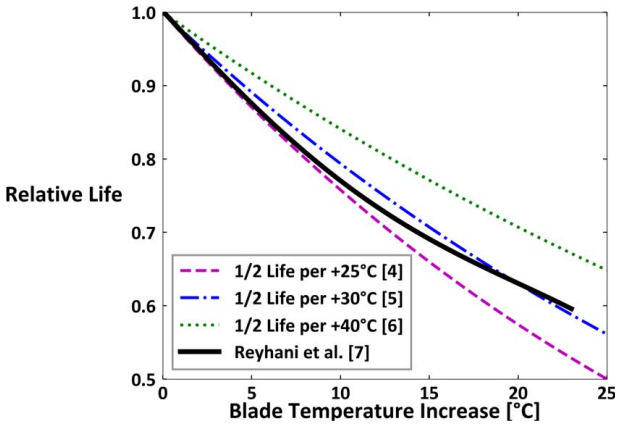

Fig. 1 Trends of relative blade life as a function of blade surface temperature increase

interaction to assess the sensitivity of blade life to factors such as thermal barrier coating (TBC) thickness, firing temperature, and engine operating load. From their analyses, a relationship was determined between blade surface temperature and blade life as shown in Fig. 1. Also shown in Fig. 1 is an assumed form of the reported first-order estimates, previously discussed, using an exponential decay function as a function of ΔT, which is the increase above the design target temperature.

$$\text{Relative Life} = a \exp\left[(1-b)\Delta T\right] \tag{1}$$

Figure 1 shows that the analysis performed by Reyhani et al. is in approximate agreement with the estimates provided by the other researchers.

The increase in blade temperature above the design temperature is caused by a range of factors including part-to-part manufacturing variations. The most comprehensive public study on the impacts of manufacturing tolerances relative to turbine cooling was conducted by Bunker [1] who investigated sensitivity to 32 manufacturing factors. In Bunker's assessment, a range of geometric factors including hole angles, orientations, spacing, and shape can each increase metal temperatures by as much as 39 °C. Bunker's study indicates that substantial thermal performance variations can occur due to variation within acceptable tolerances, and that blades must be carefully inspected to ensure cooling performance and life targets will be met for engine-run parts.

Several studies have specifically assessed film cooling performance in more detail in the presence of manufacturing defects, such as partial hole blockage due to the thermal barrier coating process. Bunker [8] investigated the impact of partial hole blockage on adiabatic effectiveness of round and shaped holes on a flat plate. The blockage reduced the centerline effectiveness of round holes by more than 50% while the shaped holes were more resilient to blockage with a near-hole reduction of 30%. A study by Sundaram and Thole [9] investigated partial hole blockage on a vane endwall and found a reduction in adiabatic effectiveness of about 30% in the worst case. A later study by Whitfield et al. [10] examined adiabatic effectiveness of cylindrical and shaped film cooling holes on a flat plate with blockage areas ranging from 29% to 52% of the exit area. The blocked cylindrical hole showed a reduction in effectiveness of 30–50% at the same pressure ratio compared to an unblocked hole. Whitfield et al. found that the cooling for shaped holes did not suffer as much as round holes due to the blockage at blowing ratios up to one, agreeing with the finding by Bunker [8]; however, at high blowing ratios, the blocked shaped holes had at least 60% lower effectiveness.

In another specific cooling hole study, the research by Haydt et al. [11] evaluated the impacts of a meter-diffuser offset for film-cooling holes, which is a potential manufacturing defect of shaped holes. They found that most meter-diffuser offsets reduced the adiabatic effectiveness, although one particular fore offset resulted in improved adiabatic effectiveness levels than even the aligned diffuser, which was the design intent. All of these studies indicate the substantial cooling performance variations possible in the presence of manufacturing variations.

A few additional studies have examined part-to-part variations in engine hardware. A dissertation by Sidwell [12] presented as-manufactured blade flow data for turbine airfoils from multiple blade rows of commercial aero engines. His study provided probabilistic analyses to estimate blade oxidation life. Using this analysis, Sidwell showed that both efficiency and life can be improved by selectively assembling blades into a blade row rather than using a random assembly. Sidwell indicated that using selective assembly when having 15% of blades at a reduced cooling flow only reduced the blade row life by 3% compared to random assembly. Conversely, using only the 15% highest-flowing blades allowed for a firing temperature increase of 140 °F (78 °C) with the same life or alternatively an 84% extension of life at the same temperature.

External airfoil shape variations also affect thermal loads and durability as shown by Duffner [13] who evaluated as-manufactured turbine vanes. The variations in airfoil shape observed on production vanes were scaled to a new vane design that was evaluated using simulations. Their simulations indicated the most critical airfoil dimension was expectedly the throat area. The variations in airfoil shape impacted the aerodynamic losses given the passage mass flowrates exceeded design tolerances. The deviations in airfoil shape impact the local heat transfer coefficients and freestream temperatures, both of which may contribute to higher heat loads and decreased blade life.

Overall, many manufacturing aspects affect blade temperature, but there have been no studies using engine parts that exhibit manufacturing variations with flow measurements and spatially-resolved temperatures at engine relevant conditions. New measurement techniques and advanced sensors are continuing to reveal information about blade thermal performance, but a substantial gap persists in the open literature linking the cooling performance and expected life of rotating blades with observed blade-to-blade manufacturing deviations. Our study addresses this gap by presenting blade-to-blade flow and thermal variations in engine hardware. Our research also extends the observed thermal variations to estimate the corresponding reduction in blade life using scaled overall effectiveness measurements. Unlike previous studies that relied on probabilistic analysis, this study uses a fully experimental approach to link the manufacturing variations to expected life variations.

Turbine Test Facility and Instrumentation

The measurements on rotating blades were collected at the Steady Thermal Aero Research Turbine (START) Laboratory at the Pennsylvania State University. The turbine test rig in START is an open-loop, continuous-duration facility that includes a one-stage turbine test section. The vane and blade hardware in the test section are true-scale and representative of those found in the high-pressure turbine of a modern aero engine. The design of the facility is described in detail by Barringer et al. [14] with several facility upgrades given by Berdanier et al. [15].

A schematic of the turbine facility and test section is shown in Fig. 2. Ambient air is pressurized by a pair of 1.1 MW (1500 HP) industrial compressors that can provide a combined output flow of 11.3 kg/s (25 lbm/s) at a pressure of up to 480 kPa (70 psia). After compression, the nominal air temperature is 395 K (250 °F). Most of the compressor exit flow is directed to the main gas path through an in-line natural gas burner that can elevate the main gas path temperature up to 672 K (750 °F) at the maximum flowrate.

A fraction of the compressed flow bypasses the burner to be used as cooling air and instead passes through a heat exchanger that

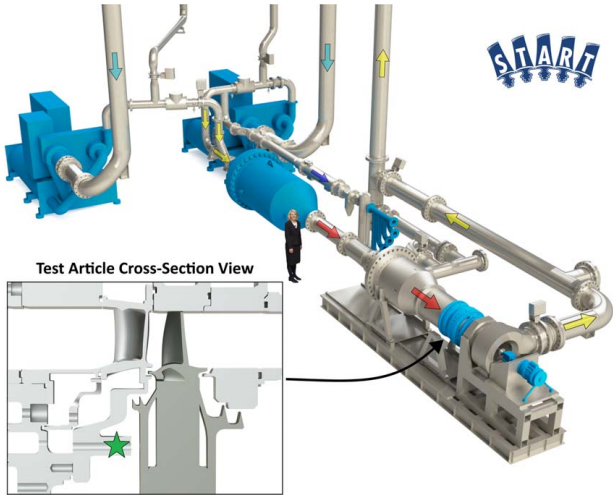

Fig. 2 START facility overview with one-stage turbine test section showing TOBI flow measurement location with a star

reduces the air temperature to 273 K (32 °F). The cooling air can be delivered to the turbine test section via three independently-controlled lines for under-platform purge flow, tangential onboard injection (TOBI) flow to cool the rotating blades, and vane trailing edge flow.

The temperature of main gas path flow entering the turbine section is measured by an array of fixed thermocouple probes at 50% span spaced circumferentially around the inlet upstream of the vanes with a variation of less than 1 °C. The TOBI flow temperature is measured on the stationary hardware at the inlet to the TOBI nozzle, marked with a star in Fig. 2. Flow network predictions indicate a change in the cooling flow temperature of less than 1 °C from the measurement location to the blade root, or less than 1% of the temperature difference between the main gas path and cooling flow temperatures.

Infrared Imaging System. The key measurement technique used for this study was infrared (IR) imaging. The IR system used in this study was custom-developed to enable spatially-resolved metal temperature measurements of blades rotating at over 10,000 rpm in the START facility. This system was introduced by Knisely et al. [16], who benchmarked the detector performance and provided guidance for implementing and operating an IR imaging system with rotating turbine blades.

The IR system consists of a mercury-cadmium-telluride quantum infrared detector that operates in the long wave IR band and is capable of capturing thermal images with integration times as low as 0.6 μs. This capability to operate at very low integration times is necessary to minimize motion blur from the rotating blades. The detector is located outside of the test section and is attached to an optical probe that inserts into a custom, additively-manufactured (AM) vane to provide visual access from the detector to the pressure side of the blade, as shown in Fig. 3. Although not shown in detail the upstream vane was specially designed through computational fluid dynamics in order not to impact the downstream blade being imaged. Using a shaft encoder signal, the camera acquisition is phase-locked to a desired position relative to a chosen blade, such that one image per revolution is collected. By adjusting the radial and yaw positions of the probe, the full pressure side and leading edge of the blade can be imaged using several views.

To minimize measurement uncertainty with IR imaging, the blades were coated with five layers of a thin, high-emissivity Krylon matte black spray paint with a total coating thickness of 0.07 mm and an emissivity of 0.92. A benchtop calibration procedure was used to calibrate the IR system at an integration time of

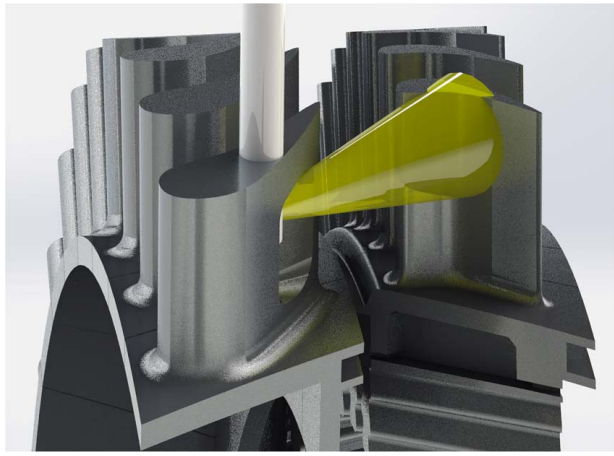

Fig. 3 Optical access to the blade's pressure side is achieved through an optical probe inserted into a custom AM vane

2.0 μs. A total of 200 phase-locked images were collected and averaged to form a representative measurement. Further details on the coating properties, calibration procedure, choice of integration time, and averaging of images are described by Knisely et al. [16].

All contributing factors to uncertainty in normalized overall effectiveness measurements were incorporated into an uncertainty analysis using the technique described by Moffat [17] to find the leading contributors and the magnitude of uncertainty. The contributors are shown in Fig. 4. With 200 images averaged, the associated sensor noise and curve fitting errors are low enough that they are not the main drivers of uncertainty, and further increasing the number of averaged images would not improve the uncertainty in overall effectiveness. Additionally, the temperature accuracy and temperature uniformity of the calibration surface were considered, although the use of high-accuracy calibrated thermocouples and a highly conductive calibration plate were used to reduce the uncertainty.

The largest contributor to uncertainty is emissivity, as the measured surface temperature is highly sensitive to variations in emissivity. The use of a high-emissivity blade coating helps reduce the contribution of background temperature, which would otherwise be the dominant contributor. Finally, the uncertainty in thermocouple measurements for cooling flow and main gas path temperatures, used to convert surface temperature to overall effectiveness, were found to contribute only moderately.

The uncertainty in effectiveness was further reduced by operating the START rig at a high main gas path temperature and a low

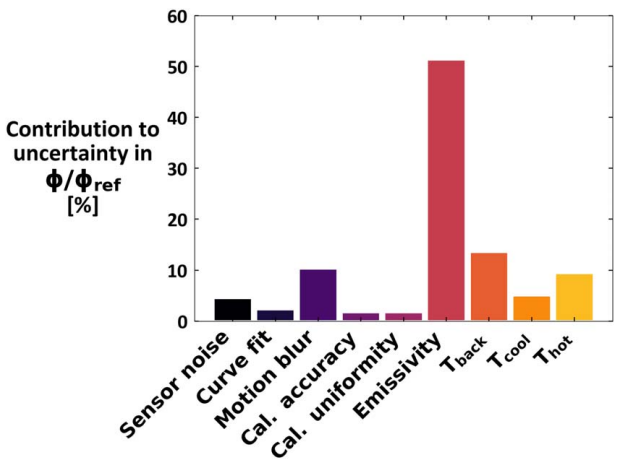

Fig. 4 Contributors to uncertainty in normalized overall effectiveness using IR measurement system

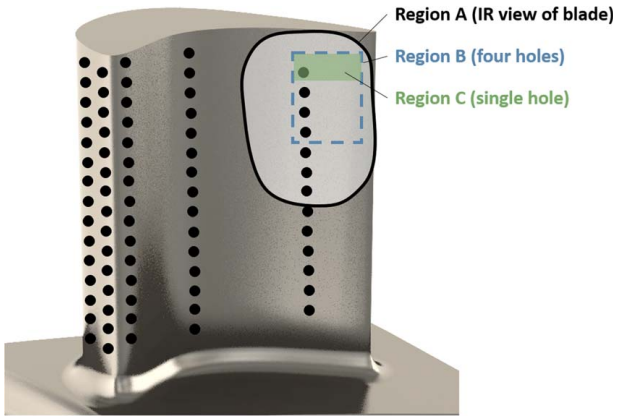

Fig. 5 Regions used for analysis with the (A) full viewing area, (B) four cooling holes, and (C) a single cooling hole

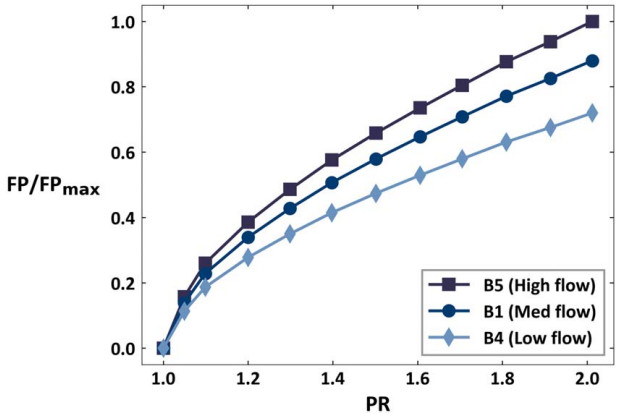

Fig. 6 Normalized flow parameter as a function of pressure ratio for three turbine blades (full blade flow)

cooling air temperature to ensure the maximum temperature difference. Based on these contributing factors, the magnitude of uncertainty in normalized overall effectiveness was 3.8% for the lowest values of normalized effectiveness and 3.9% for the highest values. Effectiveness results in this study are normalized by ϕ_{ref}, the highest effectiveness value measured at any location in Region C (as will be described) across all blades and test conditions. Repeatability in ϕ/ϕ_{ref} ranged from 0.1% to 0.9% with a median of 0.5% for the 65% cooling flow case, while repeatability in ϕ/ϕ_{ref} for the nominal flow case ranged from 0.2% to 2.5% with a median repeatability of 1.3%.

Although the IR system was used to image the entire pressure side of the blade, this paper focuses on the tip region, as shown in Fig. 5. The full field of view is labeled Region A, which is inclusive of Region B that includes the coverage area for four cooling holes and Region C that includes the coverage area for a single hole. The turbine blades used in this study include state-of-the-art compound-angle, shaped film cooling holes. These blades are all identical in their design intent, but exhibit variations in both blade flow and thermal performance due to manufacturing variations.

Blade Flow Measurements. Measurements of blade flow were used to assess the as-manufactured internal and external cooling features of turbine blades and vanes. The blade root was secured in a sealed fixture, which provided a supply plenum pressure, P_{in}, at the blade root, while the corresponding mass flowrate, $\dot{m}$, through the blade was measured using a flowmeter. The two measured variables to quantify the flow through the blade are expressed in terms of pressure ratio (PR) and flow parameter (FP), respectively.

$$\mathrm{PR} = \frac{P_{in}}{P_{out}} \tag{2}$$

$$\mathrm{FP} = \frac{\dot{m}\sqrt{T_{in}}}{P_{out}}\ (\mathrm{kg\,K^{1/2}/[Pa \cdot s]}) \tag{3}$$

In these equations, P_{out} is the room (ambient) absolute pressure and T_{in} is the absolute temperature in the plenum at the blade root. The pressure ratio is nondimensional, while the flow parameter is dimensional with units noted above. The pressure regulator and instrumentation are computer-controlled, to allow for automated testing and measurement of FP as a function of PR. Figure 6 shows example curves of FP as a function of PR for three blades that have the highest, lowest, and median flows. These curves are normalized by $\mathrm{FP_{max}}$, the flow parameter at PR = 2 for the highest flowing blade (blade 5).

As an important verification step for this study, the blades were flow tested both before and after painting. Based on measurement uncertainties, the painting process did not significantly affect blade flow for any of the blades tested. This step ensured that the paint was not restricting the blade flowrate compared to an uncoated blade.

While flowing air through the full blade can provide an overview of the blade's flow performance, an understanding of local flow performance is important to ensure an individual region of the blade is receiving sufficient cooling. The four cooling holes in Region B, shown in Fig. 5, were isolated by using wax to block all other cooling holes on the blade. Using the same blade flow rig with a regulator made for a smaller flow range, the FP through the four holes was measured at the nominal pressure ratio for several blades. Similarly, wax was then used to block three of the holes in Region B such that only the single hole in Region A was unblocked.

A detailed uncertainty analysis was conducted for blade flow measurements to ensure the observed blade-to-blade variations were statistically significant. From Eq. (3), flow parameter is a function of $\dot{m}$, T_{in}, and P_{out}, and the uncertainties of each measurement were propagated to determine the contributors to uncertainty and magnitude of uncertainty in normalized flow parameter as shown in Fig. 7.

The full blade testing was conducted with a high-range mass flowmeter, while the other two cases used a low-range mass flowmeter. The uncertainty in mass flow scales with the range of the flowmeter while the temperature and pressure measurement uncertainty are the same between the two flowmeters. As a result, the mass flow measurement is the leading contributor to uncertainty for the full blade measurements, while the mass flow contribution for the other tests is insignificant. As shown in Fig. 7, the magnitude of uncertainty in normalized FP is at most 3.0%. Uncertainty in normalized FP for the full blade tests ranged from 2.6% for the highest-

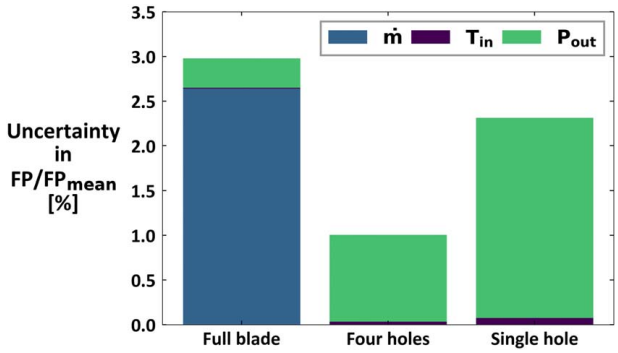

Fig. 7 Magnitude of uncertainty in normalized flow parameter for each blade section with contributors to uncertainty stacked

flowing blade to 3.0% for the lowest-flowing blade, while the uncertainty in FP through four holes ranged from 0.7% to 1.0% and single holes ranged from 1.2% to 2.3%. The uncertainty in pressure ratio is 0.7% for all cases.

Blade-to-Blade Flow Variation Results

Blade flow measurements for nine blades are shown in Fig. 8 for the three blade regions indicated in Fig. 5. The flow parameters for the full blade are normalized by the mean flow parameter through the full blade for nine blades, and the flow parameters through four holes or a single hole are similarly normalized by the mean of their group.

The blade-to-blade variations in flow parameter were found to be substantially larger than the measurement uncertainty. The airflow through a full blade, Fig. 8(*a*), varies by approximately ±15% of the mean value at the nominal pressure ratio, while larger flow variations were observed at the four-hole and single-hole resolutions. The flow through four cooling holes, Fig. 8(*b*), varies from 53% of the mean for blade 3 to 129% of the mean for blade 1 at the nominal pressure ratio. Through a single hole, Fig. 8(*c*), blade 5 flowed only 45% of the mean while blade 9 flowed 145% of the mean value—over three times as much as the same hole on blade 5.

The data presented in Fig. 8 can give the variation of flow performance within the different sections of each blade. For Figs. 8(*b*) and 8(*c*), the reference values of FP/FP_{mean} from Fig. 8(*a*) are indicated with the black symbols. From the symbols, there are substantial variations in flow for different sections of the same blade. For example, blade 9 is flowing 90% of the mean value through the full blade, 100% of the mean amount through four holes, and 145% of the mean (the highest flow) through a single hole. Conversely, blade 5 has 117% of the mean flow through the full blade but only 45% of the mean flow through a single hole.

These results illustrate how manufacturing can locally and globally affect the coolant flow distribution. The blade-to-blade flow variations imply an unequal distribution of cooling flow around the turbine wheel, which results in a circumferential variation in temperature and efficiency.

Variations in Film Cooling Trajectories

In comparing the film cooling performance on multiple rotating blades, slight variations in hole locations between blades relative to the captured image can cause the holes to appear in different locations for different blades. To quantify manufacturing effects on cooling, we chose to use the measured peak effectiveness levels, which allowed us to compare the levels of cooling as well as the trajectory of the cooling jet. A procedure was developed to objectively identify a coordinate system for the peak effectiveness levels downstream of each hole on each blade.

The method for identifying the peak effectiveness levels is illustrated in Fig. 9 using data from one hole as an example. In Fig. 9(*a*), the thermal image of the single cooling hole in Region A (Fig. 5) is shown for one blade. Based on this image, the exact position of the cooling hole outline is unknown given the conduction and adverse convection effects. An image global (X, Y) pixel coordinate system is shown in Fig. 9(*a*). For each X position, the corresponding Y-location of the pixel with highest effectiveness was identified, resulting in a series of (X, Y) coordinates for the path; this path is overlaid on the contour shown in Fig. 9(*a*). The effectiveness at each coordinate of the path is also recorded, as shown in Fig. 9(*b*). The path distance s' is calculated for the trajectory by the root-sum-square of the distances dx' and dy' for each point along the path. The position of maximum slope, $d\phi/ds'$, is identified and used to set the origin of the coordinate system. This point is expected to be related to the lower left edge of the hole along the hole axis. Figure 9(*c*) shows the result in applying this method with the identified coordinate axes and film trajectory. This procedure ensures the same blade-to-blade coordinate systems with the film trajectory originating at (0, 0) for all cases.

In developing the method for identifying the jet trajectory, other gradient-based methods of computing a coordinate system yielded similar results. In one method, the horizontal image gradient (Sobel operator [18]) was used to set the position of the vertical axis, and the point where the path of maximum effectiveness crosses that axis is set as the origin. In another similar method, a vertical image gradient instead of the horizontal gradient was also evaluated. Based on the maximum differences in origin position between these three methods, overall positioning uncertainty for the coordinate system is estimated to be ±0.5 metering hole diameters. Ultimately, the method using the gradient along the path was

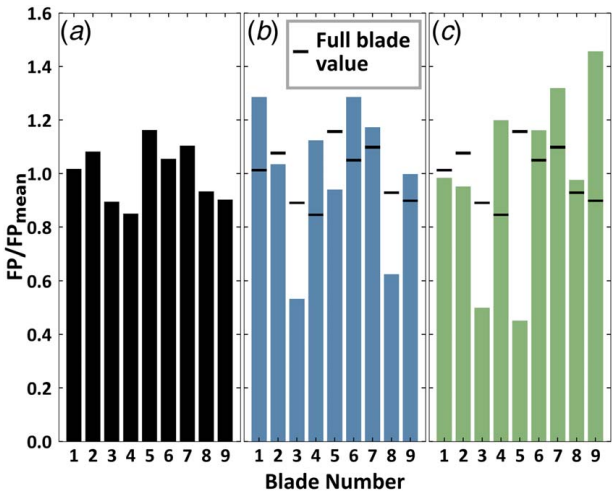

Fig. 8 Flow parameter measurements for nine blades for (*a*) the full blade, (*b*) four holes in Region B, and (c) the single hole in Region C; results normalized by mean of each group

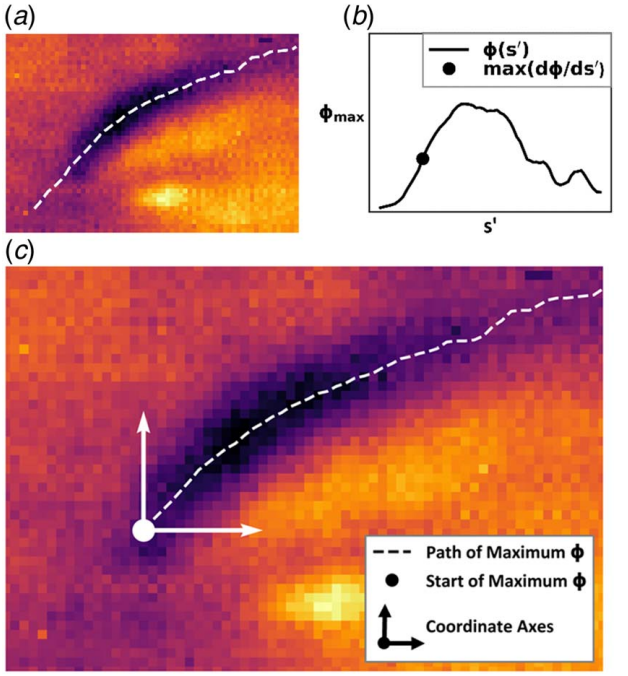

Fig. 9 Process used to define coordinate system for defining coolant jet trajectories: (*a*) thermal image of cooling hole with path of maximum effectiveness overlaid, (*b*) effectiveness as a function of path distance with the point of maximum slope identified, and (c) original thermal image showing origin, coordinate system, and path of maximum effectiveness

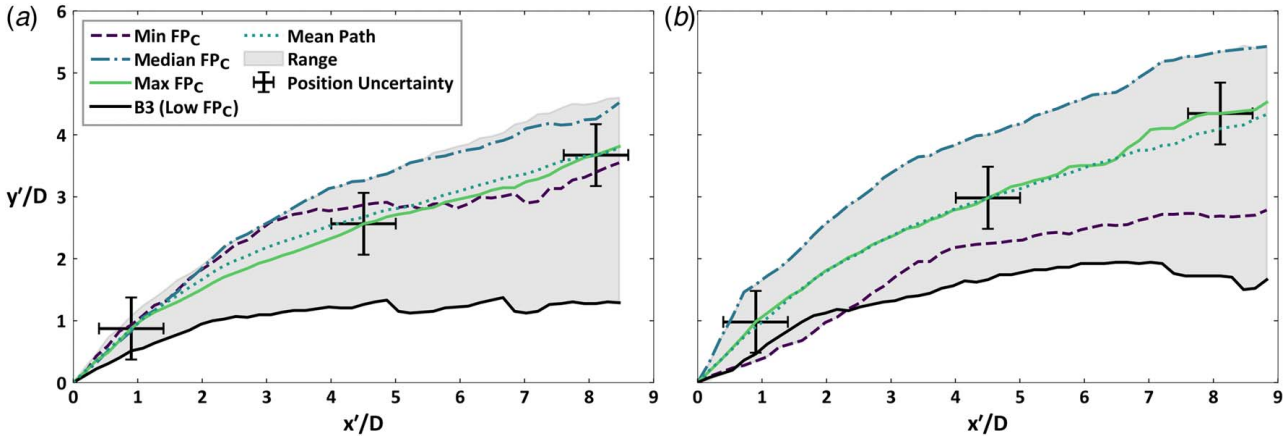

Fig. 10 Range of film cooling trajectories among nine different blades with holes with highest, lowest, and median flow parameter blades identified along with the mean path and uncertainty in positioning: (*a*) at 65% of nominal cooling flow and (*b*) at nominal cooling flow

chosen because higher temperature gradients occurred along the path compared to the other methods. As the coordinate system defined in this study is computed from the image data and not aligned with the physical hole edges, positions in x, y, and s will be denoted with a prime ($'$) throughout the discussion of film trajectories, although the coordinates are expected to be related to the edges of the hole.

In using the method for establishing the coordinate system for each cooling hole, the trajectories of the jets on different blades (described by the path of maximum effectiveness) can be compared. Figure 10(*a*) shows the trajectories when the blades are supplied with 65% of the nominal design cooling flow while Fig. 10(*b*) is at the nominal blade flowrate. The filled region represents the variation in trajectories from the nine blades for a single hole (Region C in Fig. 5) with the blades having the maximum, minimum, and median flow parameters shown, as discussed in Fig. 8. Note that these blades were selected based on flow parameter and not flowrate, but the flow parameter scales directly with flowrate because the flow parameters were measured at the same pressure ratio. The positioning uncertainty of ±0.5 diameters is also shown, which estimates the maximum error in relative positioning of each path. The hole breakout extends approximately 3.5 diameters in the x'- and y'-directions. The mean trajectory was calculated based on the mean y'/D value of all nine blades at each x'/D value.

The majority of the trajectories of the maximum effectiveness for the 65% nominal cooling flow were similar, as shown in Fig. 10(*a*), as the blades with the minimum, median, and maximum flow parameters have similar trajectories to the mean path. There was one hole, however, on blade 3 that was identified to have a significantly different trajectory by as much as three hole diameters in the y'-direction. Although blade 3 and the blade labeled Min FP_C have similar flow parameters for a given pressure ratio through a single hole, the resulting film trajectories vary substantially. As such, these results imply that there were hole manufacturing features affecting the trajectory (rather than flow differences) for the hole on blade 3 relative to the median trajectory for the other holes.

For the nominal cooling flow case, Fig. 10(*b*) shows a much wider variation in trajectories between different blades relative to the 65% cooling flow implying that cooling performance is more sensitive to manufacturing differences at high cooling flows. The two lowest-flowing blades, Min FP_C and blade 3, show similar trajectories where maximum effectiveness levels are as much as four hole diameters below that of the trajectory from the median-flowing blade. While the lowest-flowing blade had the trajectory with the lowest y' values, the highest-flowing blade did not have the trajectory with the highest y' values. As shown in Fig. 10(*b*), the blade with the highest flow (Max FP_C) had a trajectory more centered between the low-flow blades and the median-flow blade (Median FP_C).

The median-flow blade (Median FP_C) had the highest trajectory as indicated by the highest y'/D values for a given streamwise position, indicating that potentially other manufacturing variations, such as hole shape have a role in dictating the blade-to-blade variations in the jet trajectory for the maximum effectiveness. For median-flow and high-flow blades, the variations in trajectories are not explained by flow parameter measurements alone.

At both cooling flowrates shown in Figs. 10(*a*) and 10(*b*), variations in trajectories were observed even between blades that flowed similarly. With such a variation in coverage area for cooling air, there is a potential for hot spots to occur that result in reduced blade life. Additionally, this result has implications for blade design and hole spacing. Given the range of trajectories, the cooling hole spacing is made difficult to determine for the airfoils tested without considering these manufacturing variations. In addition to observed blade-to-blade differences in film trajectory, variations in overall effectiveness along the trajectory were observed. These effectiveness variations are expected to be related to blade flow parameters, as discussed in the next section.

Correlating Effectiveness With Blade Flow

While the trajectory of the maximum cooling effectiveness describes its spatial path, additional information can be gained by evaluating the variation in the cooling effectiveness along that trajectory. In a manner similar to Fig. 10, the range of maximum effectiveness values as a function of path distance s'/D is shown in Fig. 11(*a*) for the 65% cooling flow and in Fig. 11(*b*) for the nominal cooling flow cases. The effectiveness values are normalized by a reference value corresponding to the maximum effectiveness value along the path at the nominal cooling flow case.

The filled areas in Fig. 11 represent the ranges of effectiveness values for each cooling flow case, and effectiveness is shown for individual blades with maximum and minimum flow parameters through a single hole (Max FP_C and Min FP_C) and maximum, minimum, and median flow through four holes (Max FP_B, Min FP_B, and Median FP_B).

Figure 11(*a*) shows a blade-to-blade variation in maximum effectiveness of approximately 10% at the 65% flow case. The amount of flow through a single hole influences effectiveness only slightly, as Max FP_C and Min FP_C show maximum effectiveness values within 3% of each other. The flow through four holes is a larger driver of maximum effectiveness, with Min FP_B showing effectiveness levels 7–10% lower than Max FP_B.

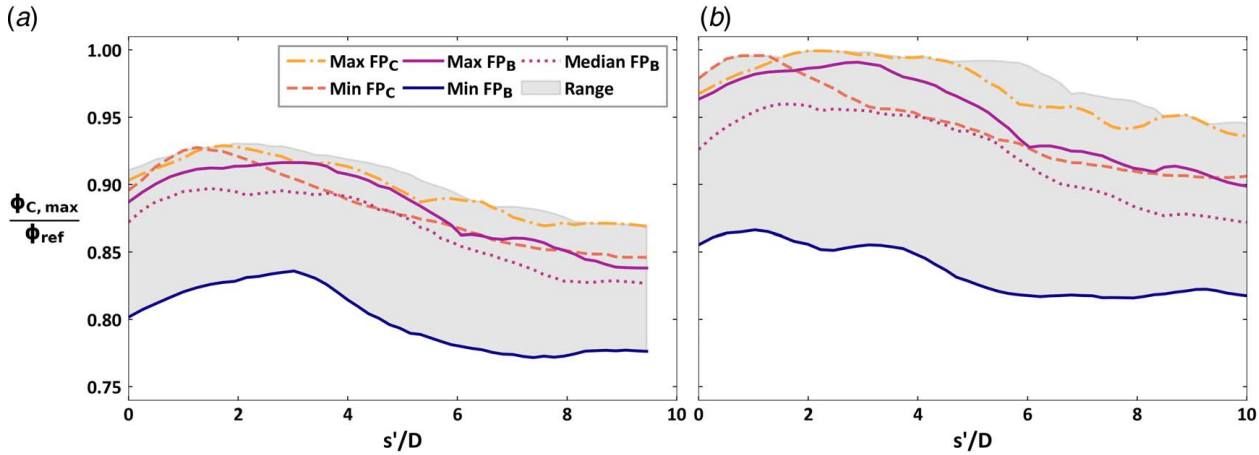

Fig. 11 Range of normalized effectiveness downstream of the hole in Region A as a function of path distance with the highest and lowest flowing blades in Regions C and B identified as well as the median-flowing blade in Region B: (*a*) at 65% of nominal cooling flow and (*b*) at nominal cooling flow

At the nominal cooling case, shown in Fig. 11(*b*), the blades with the maximum and minimum flow through a single hole (Max FP$_C$ and Min FP$_C$, respectively) have effectiveness values within 5% of each other, despite Min FP$_C$ flowing only 1/3 as much air as Max FP$_C$ through the hole of interest. The blades with the maximum and minimum flow through four holes (Max FP$_B$ and Min FP$_B$, respectively) vary in effectiveness substantially more at a 10–15% difference.

Comparing the 65% flow case in Fig. 11(*a*) to the nominal flow case in Fig. 11(*b*), the blade-to-blade variation in effectiveness increases with flowrate, further indicating that cooling effectiveness is more sensitive to manufacturing variations at high cooling flowrates.

In addition to studying cooling effectiveness downstream of the hole, area-averaged effectiveness is used to assess the average performance of each blade in a particular region and correlate with blade flow data. Figure 12 shows the normalized area-averaged overall effectiveness as a function of normalized flow parameter for the three blade regions and two flowrates, with each point representing a single blade. Effectiveness in each subplot of Fig. 12 is normalized by the same ϕ_{ref} value from Fig. 11, while flow parameters are normalized by the mean of the region, as presented in Fig. 8. Figures 12(*a*)–12(*c*) present effectiveness measurements at the 65% cooling flow case, while Figs. 12(*d*)–12(*f*) show effectiveness at the nominal cooling flowrate.

Figure 12(*a*) shows the normalized area-averaged effectiveness in Region A at 65% cooling flow as a function of the full-blade normalized flow parameter. Given that only a small portion of the total blade flow is a part of Region A with the flow distribution throughout the blade, these values are not expected to be strongly correlated. As shown, there is substantial scatter, and the full-blade flow performance is not a good indicator for thermal performance in a more specific region of the blade.

Figure 12(*b*), flow parameter and overall effectiveness of the four holes in Region B are found to be more tightly correlated than in Region A. As flowrate increases, effectiveness also increases, with notable differences in thermal performance between the highest- and lowest-flowing blades. The two blades with the lowest flow through four holes have 7–9% lower effectiveness compared to those with the highest flow. This detailed flow data show that thermal performance can be closely tied to flow variations.

The most detailed region is shown in Fig. 12(*c*), where the overall effectiveness in Region C is shown as a function of flow parameter through the single hole. Despite the more scattered data in Fig. 12(*c*) compared to Fig. 12(*b*), there is still a trend of increasing effectiveness as flow parameter increases; however, some blades such as 5 and 9 seem to be exceptions to the trend. An explanation for these two points can be found by comparing the measured blade flow trends for these two blades from Fig. 8. For blade 5, the flow through a single hole is very low, but the flow through four holes is average, so the adjacent holes are able to compensate with conduction and strong internal cooling. In other words, one poor performing cooling hole does not ruin the local performance. For blade 9, the flow through a single is very high, but the flow through four holes is average. For blade 9, a single hole with exceptionally high flow does not seem to notably improve the effectiveness.

Comparing the nominal flow cases in Figs. 12(*d*)–12(*f*) to the corresponding 65% flow cases in Figs. 12(*a*)–12(*c*), respectively, the increase in flow results in a uniform increase in effectiveness of 5–6% for each blade and for each region. With each blade showing the same increase in effectiveness for a given increase in flow, effectiveness scales similarly for each blade as a function of cooling flowrate.

Overall, the flow performance of adjacent holes is a key factor contributing to the local thermal performance, and the local flow parameter through four adjacent holes is better correlated with local effectiveness than flow through a single hole. The use of spatially-resolved measurements with IR, as opposed to point sensors, is crucial to track the cooling jet trajectories and quantify the area-averaged effectiveness. With the observed blade-to-blade variations in overall effectiveness, significant variations in component life would be expected if these blades were operating at engine conditions.

Scaling Thermal Variations to Engines

The variations in area-averaged effectiveness were scaled to engine conditions by assuming design values for the first-stage high-pressure turbine blade in the NASA E^3 gas turbine engine [19], shown in Table 1. Note that the surface-averaged overall effectiveness was not given in the report, but the effectiveness value of 0.48 is estimated based on the average temperature of 22 surface nodes at 50% blade span. These values in Table 1 are conservative by modern standards; many newer engines are designed for higher temperatures and higher effectiveness.

Using the normalized variation in effectiveness in Region B from Fig. 12(*b*), the design values from Table 1, and the definition of overall effectiveness, ϕ,

$$\phi = (T_\infty - T_s)/(T_\infty - T_c) \tag{4}$$

the blade-to-blade temperature variation was calculated and is shown in Fig. 13. The blade with the highest effectiveness,

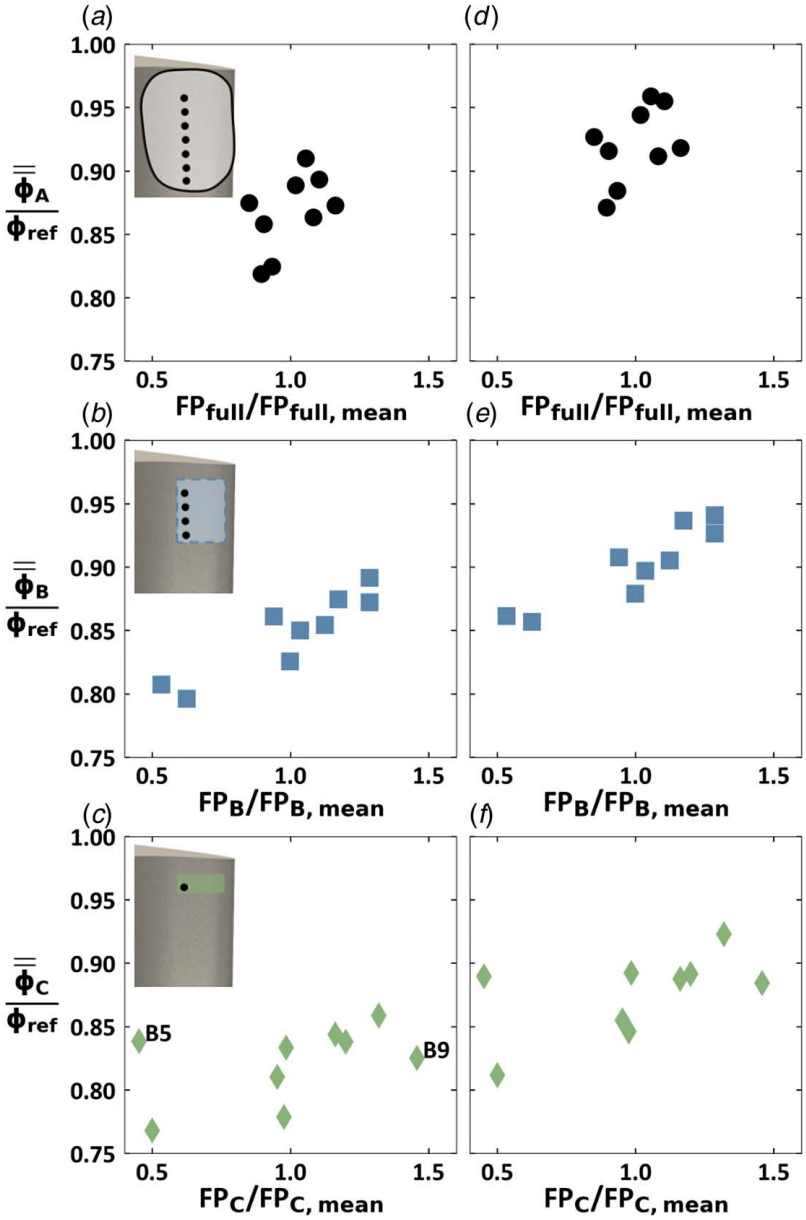

Fig. 12 Normalized area-averaged overall effectiveness as a function of normalized flow parameter: (*a*) Region A at 65% cooling flow, full blade, (*b*) Region B at 65% cooling flow, four hole, (*c*) Region C at 65% cooling flow, single hole, (*d*) Region A at nominal cooling flow, full blade flow, (*e*) Region B at nominal cooling flow, four hole, and (*f*) Region C at nominal cooling flow, single hole

blade 6, is set as the baseline scaled temperature value, as all other blades have a higher temperature. By this method, a temperature difference of up to 33 °C is shown across the nine blades analyzed in Fig. 13.

The models for lifing provided in and summarized in Fig. 1 provided a first-order estimate for evaluating the results shown in Fig. 13. Using a relationship for blade life as a function of surface temperature, the blade-to-blade variations in surface temperature can be converted to variations in life. Similar conclusions would be drawn even if the designer chooses a different functional relationship between life and surface temperature.

Estimated blade-to-blade variations in life are shown in Fig. 14. The bars themselves assume a 50% reduction in life for a 30 °C increase in surface temperature [5], while the error bars represent the range of potential life values based on an increase in surface temperature of 25–40 °C reducing life by 50% (representing the range of functions in Fig. 1). As the blade with the highest temperature variation, blade 8 is expected to last about 47% as long as the best performer, blade 6. With these substantial variations in life solely due to thermal performance variations, the part-to-part variations when considering manufacturing effects are important to the expected part life. If the worst-performing blade is able to achieve the nominal life target, the best-performing blades such as blade 6 can achieve more than 100% longer life, representing a substantial cost savings for replacement intervals.

Table 1 Design values for scaling to engine [19]

Specification	Design value
Blade inlet temperature, T_∞	1396 °C (2545 °F)
Cooling air temperature, T_c	628 °C (1162 °F)
Blade overall effectiveness, ϕ	0.48

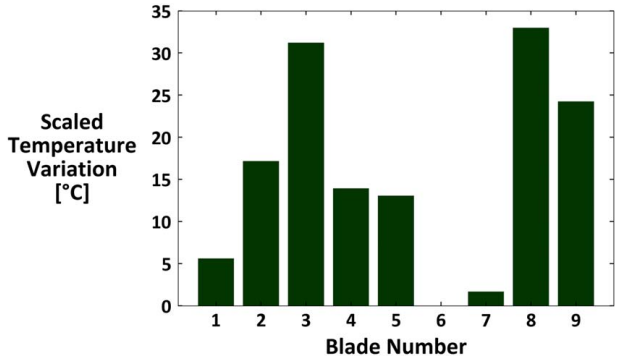

Fig. 13 Scaled blade-to-blade temperature variation expected at engine conditions

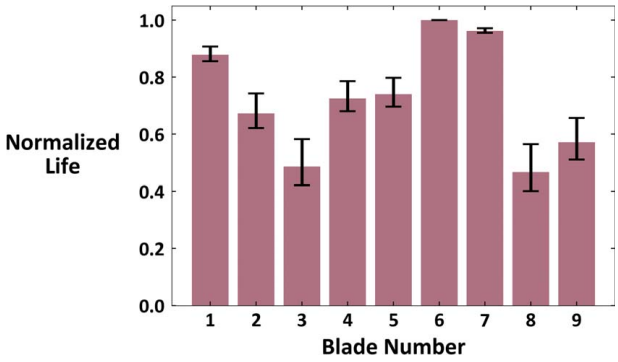

Fig. 14 Normalized life variation expected due to blade-to-blade variations in temperature assuming a surface temperature increase of 30 °C reduces life by 50% [5]

Conclusions

Robust design of gas turbines requires an understanding of the variations inherent in manufactured parts with tolerances, using statistics to ensure all parts meet life requirements. Experimental measurements on turbine hardware with the same nominal design are needed to bound the variations in manufacturing factors. Blade-to-blade variations in flow and overall cooling effectiveness were measured for nine modern, cooled turbine blades. A blade flow bench was used to measure flow through each full blade as well as through four holes and a single hole on each blade, while infrared thermography was used to measure overall effectiveness on the blade pressure side.

The spatially-resolved nature of thermal measurements with IR imaging enabled the study of cooling jet trajectories and area-averaged effectiveness on rotating blades. The trajectories of film cooling jets exiting a compound-angle shaped hole on nine different blades were compared. The trajectory of a jet exiting a low-flowing hole is swept in the mainstream flow direction, while jets with moderate or high flow have trajectories more aligned with the compound angle. Even among holes with similar flow, the film trajectories can vary substantially indicating the importance of specific hole features that may vary due to manufacturing. Additionally, both film trajectories and maximum effectiveness were found to vary more at high cooling flows.

Internal cooling is a strong contributor to overall cooling effectiveness; a single low-flowing cooling hole does not adversely affect the local cooling effectiveness, and likewise, a single high-flowing cooling hole does not notably increase the local effectiveness. The local effectiveness is most correlated with the flowrate through four neighboring cooling holes in the region of interest.

Overall effectiveness results were scaled to engine conditions to evaluate the impact on part life using simple first-order estimates. The hottest blade would be expected to survive only 47% as long as the coolest blade, despite all blades having the same nominal design.

It is important to note that this research is the first step to further detailed analyses including how the manufacturing defects of specific internal features and upstream rows of holes can affect localized cooling. However, from a global view, this initial step indicates the importance of continued investigations. To substantiate this direction, this paper showed substantial variations in both blade flow and overall effectiveness as a result of blade-to-blade manufacturing variations.

Acknowledgment

The authors would like to thank Pratt & Whitney and the U.S. Department of Energy—National Energy Technology Laboratory for sponsoring research presented in this paper. This paper is based upon work supported by the Department of Energy under Award Number DE-FE0025011. This report was prepared as an account of work sponsored by an agency of the United States Government. Neither the United States Government nor any agency thereof, nor any of their employees, makes any warranty, express or implied, or assumes any legal liability or responsibility for the accuracy, completeness, or usefulness of any information, apparatus, product, or process disclosed, or represents that its use would not infringe privately owned rights. Reference herein to any specific commercial product, process, or service by trade name, trademark, manufacturer, or otherwise does not necessarily constitute or imply its endorsement, recommendation, or favoring by the United States Government or any agency thereof. The views and opinions of authors expressed herein do not necessarily state or reflect those of the United States Government or any agency thereof.

Conflict of Interest

There are no conflicts of interest.

Data Availability Statement

The datasets generated and supporting the findings of this article are obtainable from the corresponding author upon reasonable request.

Nomenclature

D = diameter of film cooling hole
P = absolute pressure
T = temperature
X = global horizontal coordinate in image (pixels)
Y = global vertical coordinate in image (pixels)
$\dot{m}$ = mass flowrate
s' = path distance along cooling jet trajectory
x' = axial distance downstream of cooling hole
y' = radial distance from cooling hole edge
a, b = coefficients for curve-fitting
FP = flow parameter $\left(\dot{m}\sqrt{T_{\text{in}}}/P_{\text{out}}\right)$
PR = pressure ratio $(P_{\text{in}}/P_{\text{out}})$

Greek Symbols

Δ = difference
σ = Stefan–Boltzmann constant $\cong 5.67 \times 10^{-8}$ W/m^{2}K^4
ϕ = overall effectiveness $(T_\infty - T_s)/(T_\infty - T_c)$
ω = rotation rate (rad/s)

Subscripts and Accents

s = blade surface
in = inlet
max = maximum flow parameter of all blades at PR = 2.0

mean = mean flow parameter for a given blade section
out = outlet
ref = reference, maximum effectiveness value measured
∞ = freestream condition
$^{=}$ = area-averaged value

References

[1] Bunker, R. S., 2009, "The Effects of Manufacturing Tolerances on Gas Turbine Cooling," ASME J. Turbomach., **131**(4), p. 041018.
[2] Reinman, G., Ayer, T., Davan, T., Devore, M., Finley, S., Glanovsky, J., Gray, L., et al., 2012, "Design for Variation," Qual. Eng., **24**(2), pp. 317–345.
[3] Balevic, D., Burger, R., and Forry, D., 2004, "Heavy-Duty Gas Turbine Operating and Maintenance Considerations," GE Energy Report GER-3620K. p. 5.
[4] Bogard, D. G., and Thole, K. A., 2006, "Gas Turbine Film Cooling," J. Propuls. Power, **22**(2), pp. 250–270.
[5] Han, J.-C., and Wright, L. M., 2006, "Enhanced Internal Cooling of Turbine Blades and Vanes," *Gas Turbine Handbook*, R. Dennis, ed., Department of Energy, National Energy Technology Laboratory, Morgantown, WV, p. 321.
[6] Bunker, R. S., Dees, J. E., and Palafox, P., 2014, "Impingement Cooling in Gas Turbines," *Impingement Jet Cooling in Gas Turbines*, R. Amano and B. Sundén, eds., WIT Press, Southampton, UK, pp. 25–26.
[7] Reyhani, M. R., Alizadeh, M., Fathi, A., and Khaledi, H., 2013, "Turbine Blade Temperature Calculation and Life Estimation—A Sensitivity Analysis," Propuls. Power Res., **2**(2), p. 158.
[8] Bunker, R. S., 2000, "Effect of Partial Coating Blockage on Film Cooling Effectiveness," 2000-GT-0244, pp. 6–7.
[9] Sundaram, N., and Thole, K. A., 2007, "Effects of Surface Deposition, Hole Blockage, and Thermal Barrier Coating Spallation on Vane Endwall Film Cooling," ASME J. Turbomach., **129**(3), pp. 606–607.
[10] Whitfield, C. A., Schroeder, R. P., Thole, K. A., and Lewis, S. D., 2015, "Blockage Effects From Simulated Thermal Barrier Coatings for Cylindrical and Shaped Cooling Holes," ASME J. Turbomach., **137**(9), p. 091004.
[11] Haydt, S., Lynch, S., and Lewis, S., 2017, "The Effect of a Meter-Diffuser Offset on Shaped Film Cooling Hole Adiabatic Effectiveness," ASME J. Turbomach., **139**(9), p. 091012.
[12] Sidwell, C. V., 2004, "On the Impact of Variability and Assembly on Turbine Blade Cooling Flow and Oxidation Life," Doctoral Dissertation, Massachusetts Institute of Technology, Cambridge, MA, pp. 1–60.
[13] Duffner, J. D., 2008, "The Effects of Manufacturing Variability on Turbine Vane Performance," Master's Thesis, Massachusetts Institute of Technology, Cambridge, MA, pp. 1–73.
[14] Barringer, M., Coward, A., Clark, K., Thole, K. A., Schmitz, J., Wagner, J., Alvin, M. A., Burke, P., and Dennis, R., 2014, "The Design of a Steady Aero Thermal Research Turbine (START) for Studying Secondary Flow Leakages and Airfoil Heat Transfer," GT2014-25570, p. 5.
[15] Berdanier, R. A., Monge-Concepción, I., Knisely, B. F., Barringer, M. D., Thole, K. A., Grover, E. A., and Scire, J. J., 2019, "Scaling Sealing Effectiveness in a Stator—Rotor Cavity for Differing Blade Spans," ASME J. Turbomach., **141**(5), p. 051007.
[16] Knisely, B. F., Berdanier, R. A., Thole, K. A., Haldeman, C. W., Markham, J. R., Cosgrove, J. E., and Carlson, A. E., 2021, "Acquisition and Processing Considerations for Infrared Images of Rotating Turbine Blades," ASME J. Turbomach., **143**(4), p. 041013.
[17] Moffat, R. J., 1988, "Describing the Uncertainties in Experimental Results," Exp. Therm. Fluid Sci., **1**(1), pp. 5–17.
[18] Pratt, W. K., 2013, *Introduction to Digital Image Processing*, Wiley-Interscience, Hoboken, NJ.
[19] Halila, E. E., Lenahan, D. T., and Thomas, T. T., 1982, "Energy Efficient Engine: High Pressure Turbine Test Hardware Detailed Design Report," NASA CR-167955. Cincinnati, OH, p. 47.